STUDIA UBB CHEMIA, LVI, 1, 2011

THE INFLUENCE OF TiO_2 NANOPARTICLES ON MORPHO-STRUCTURAL AND ANTI-CORROSION PROPERTIES OF ELECTRODEPOSITED Zn-Ni COATINGS

DIANA BLEJAN[a], DANIEL MARCONI[b], AUREL POP[b], LIANA MARIA MURESAN[a*]

ABSTRACT. Composite Zn-Ni coatings incorporating TiO_2 nanoparticles were obtained by electrodeposition on steel from alkaline solution containing triethanolamine (TEA) as complexing agent for Ni^{2+} and polyethyleneglicol (PEG) in combination with vanillin, as leveling/brightening agents. The influence of TiO_2 nanoparticles on phase composition and structure of Zn- Ni coatings were investigated by X-ray diffraction and SEM-EDAX methods. By using polarization measurements, the corrosion behaviour of the nanocomposite coatings was examined and the corrosion process on Zn-Ni-TiO_2 composite coatings was found to be slower than on pure Zn-Ni surface.

Keywords: *Corrosion; Electrodeposition; Zinc-Nickel alloy; alkaline electrolyte*

INTRODUCTION

Considerable efforts have been devoted over the years to provide improved corrosion protection to metallic surfaces. Zn alloys with Ni have attracted much attention because Zn-Ni coatings possess higher corrosion resistance and better mechanical characteristics than pure zinc and other zinc alloy coatings [1-4]. Corrosion studies have also indicated that Zn-Ni alloys may be useful as a substitute for cadmium deposits in marine environments [5].

A relatively recent way for enhancing the corrosion resistance of zinc coatings consists in generating composite layers by electrolysis of plating solutions in which micron or sub-micron size inert particles (i.e. TiO_2, Al_2O_3 etc.) are suspended [6,7]. The electrodeposition of metallic coatings containing inert particles produces corrosion resistant coatings with enhanced mechanical and tribological properties. The advanced physical properties of composite coatings quickly became clear during the 1990s, when new areas such as electrocatalysis and photoelectrocatalysis were considered [8]. However, till now, there are only few papers focused on zinc-nickel composite coatings incorporating nanoparticles [9].

[a] *Department of Physical Chemistry, Babes-Bolyai University, 11 Arany Janos St., 400028 Cluj-Napoca, Romania*
[b] *Department of Physics, Babes-Bolyai University, M. Kogalniceanu St.1, 400084 Cluj-Napoca, Romania *limur@chem.ubbcluj.ro*

In this context, the aim of this work is to investigate the combined effect of Ni and TiO_2 nanoparticles on the corrosion resistance of zinc coatings. Zn-Ni and Zn-Ni-TiO_2 coatings were obtained by electrodeposition from an alkaline bath containing triethanolamine (TEA) as complexing agent for Ni^{2+} and polyethyleneglicol (PEG) in combination with vanillin, as leveling/ brightening agents, selected based on our previous work [10].

X ray diffraction (XRD) and SEM-EDAX methods were used to determine the structure and the surface topography of the deposits. Polarization measurements were carried out in order to characterize the corrosion behavior of the coatings by using Tafel method.

RESULTS AND DISCUSSION

Electrodeposition

As it can be seen from the polarization curves recorded during the electrodeposition of Zn-Ni coatings (Fig. 1), no significant changes are observed in the kinetically controlled region of the curves, when adding TiO_2 nanoparticles or when modifying their concentration, while a slight increase of the current density is noticed in the mixed-control region. This could be due to a catalytic phenomenon initiated by defects and dislocations or to chemical heterogeneities generated in the metallic matrix by the embedded particles at high overpotentials.

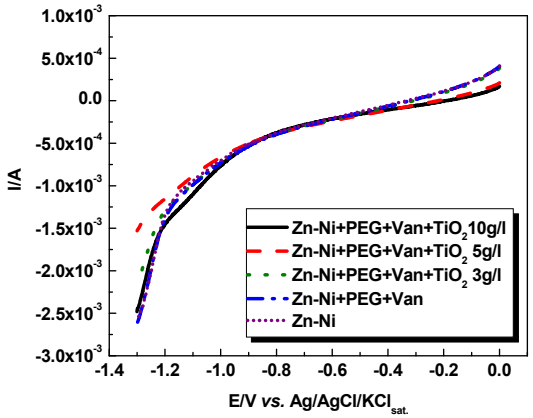

Figure 1. Polarization curves obtained during Zn-Ni electrodeposition in the absence and in the presence of TiO_2 nanoparticles.

Structural and morphological analysis

Figure 2 shows XRD pattern for four Zn-Ni coated samples: S_{01} (in the absence of brightening agents and of TiO_2), S_0 (obtained in the presence of brightening agents but in the absence of TiO_2), S_5 and S_{10} (obtained in the presence of brightening agents and with 5 g/l and 10 g/l TiO_2 nanoparticles, respectively, in the plating bath).

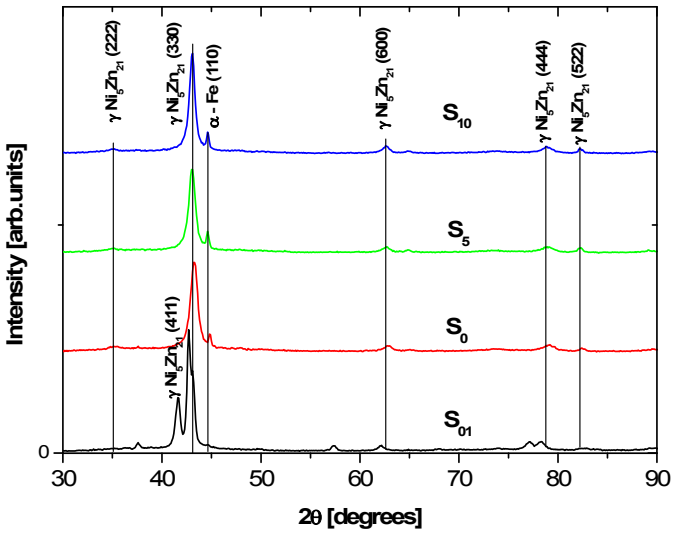

Figure 2. XRD of samples S_{01} (in the absence of brightening agents and of TiO_2), S_0 (in the absence of TiO_2 nanoparticles, x=0), S_5 and S_{10} (for x = 5 g/l and x = 10 g/l TiO_2 nanoparticles).

As can be seen from figure 2, the diffraction peaks for all samples obtained by using brightening agents and TiO_2 nanoparticles correspond only to γ-phase (Ni_5Zn_{21}). It is well-known that, the high corrosion resistance of the Zn–Ni coatings might primarily be attributed to the existence of this phase. The absence of TiO_2 peaks in the XRD spectra suggests that the concentration of phases associated with the nanoparticles is under the limit of detection of XRD method. The obtained results are in accordance with those reported for alloys containing 19–20 at. % Ni [11] and with the zinc–nickel phase diagram for γ-Ni_5Zn_{21} [12].

Another aspect that should be emphasized is related to the crystal orientation in the deposit, which is considered to be an important factor in the corrosion process. It is common knowledge that the intensity of XRD peaks (characterized by Miller indices (hkl)) is proportional to the density of oriented lattice planes. Consequently, the change of the grain orientations in presence of nanoparticles is indicated by changes of peak intensities. In the same time, the metal local coordination is correlated with planar packing densities.

In the case of investigated Zn-Ni coatings, the small change in the intensities ratio $I_{(330)}/(I_{(330)}+I_{(600)})$, presented in Table 1, shows the absence of textural modifications of deposits in the presence of TiO_2 nanoparticles. The packing density decreased in this order: ρ (110) > ρ (100), as in reference [13]. The high value of the intensities ratio $I_{(330)}/(I_{(330)}+I_{(600)})$ suggests a good packing

density associated to more closely packed (330) (or (110)) planes. The XRD pattern of sample S_{10} is similar with the result reported for pure γ-phase deposits obtained from alkaline solutions [14].

Previous investigations using XRD [15] indicated that deposition of bcc zinc–nickel on a mild steel substrate with a {110} texture resulted initially in the nucleation of {110} orientated grains of bcc zinc–nickel at the substrate/ deposit interface. Because the mild steel substrate has a {110} texture and the interplanar spacing of the mild steel {110} and of the zinc–nickel {330} are almost identical, the nickel and zinc atoms in the bcc {110} planes can fit very closely to the recesses between atoms in the mild steel {110}. This process explains the high value of $I_{(330)}/(I_{(330)}+I_{(600)})$ ratio in our samples.

Crystallite size calculations were made by using the full width at half maximum (FWHM) of (110) peak, in the Scherer equation:

$$D = \frac{0,9\lambda}{B\cos\theta}$$

where *D* is the grain size [nm], $\lambda = \lambda_{CuK\alpha 1} = 0,15406$ nm), *B* is the line width and θ is the position for (110) peak. For all coatings, the profile of (110) peak exhibits Lorentz type behavior

The calculated value for D (see Table 1) shows that the grain size decreases with increasing concentration x of TiO_2 nanoparticles up to 5g/l TiO_2, and slightly increases for x =10 g/l. The decrease of grain dimensions is due to the fact that the nanoparticles influence the competitive formation of metal nuclei and crystal growth. The TiO_2 nanoparticles disturb the regular growth of metallic crystals and causes new nucleation sites to appear.

Table 1. Parameters obtained from XRD and EDAX measurements.

Sample	$\frac{I_{(330)}}{I_{(330)}+I_{(600)}}$ %	D [nm]	Ni wt.%
S_{01}	92	14.0	15.7
S_0 (x=0 g/l TiO_2)	94	11.4	16.0
S_5 (x=5 g/l TiO_2)	95.5	10.7	16.5
S_{10} (x=10 g/l TiO_2)	95	11.9	17.0

Morphological observation of Zn-Ni nanocomposite coatings and their chemical composition were carried out by SEM and EDAX methods. Figure 3 shows the scanning electron micrographs of Zn–Ni deposits with different concentration of TiO_2 nanoparticles.

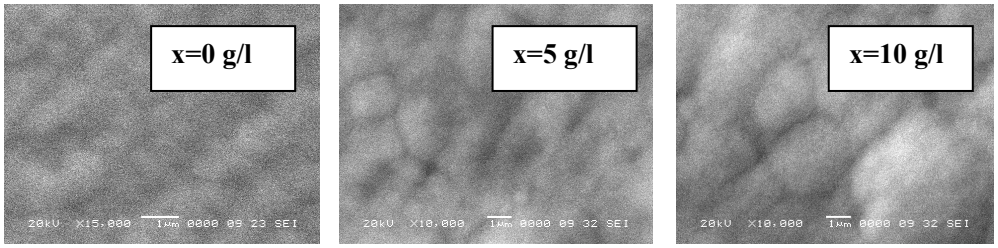

Figure 3. SEM micrographs of the Zn–Ni deposits, showing the change of morphology with TiO_2 nanoparticle concentration.

Thus, the plate-like shape morphology of the electrodeposits slowly changes by increasing the concentration x of TiO_2 nanoparticles. Similar results were obtained by Felloni *et al.* [16], who found that the platelet-type grains are closely related to the (330) (or (110)) component, and the pyramidal microstructure coincided with a preferential (600) orientation. The crystallographic preference for the (330) orientation that occurs in the presence of TiO_2 nanoparticles coincides with the formation of platelet-type structures.

Figure 4 shows the results of EDAX analysis for Zn-Ni alloy samples with x = 0 g/l, 5 g/l and 10 g/l TiO_2, respectively. The corresponding Ni content in the deposits (wt %) is presented in Table 1.

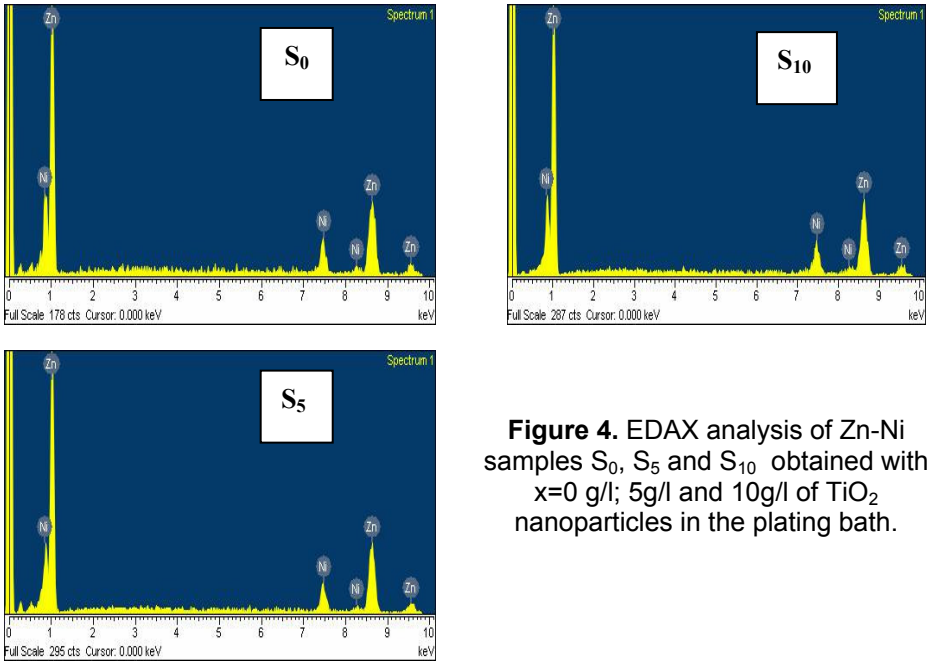

Figure 4. EDAX analysis of Zn-Ni samples S_0, S_5 and S_{10} obtained with x=0 g/l; 5g/l and 10g/l of TiO_2 nanoparticles in the plating bath.

It was observed that the Ni content increases from 16% to 17% with increasing concentration of TiO_2 nanoparticles. Literature reports mention that Ni–Zn alloy coatings on Fe substrates are relatively rich in Ni at the substrate/ deposit interface [17].

Electrochemical corrosion measurements

Open circuit potential

The open-circuit potentials (*ocp*) evolution in time for Zn-Ni and Zn-Ni-TiO_2 samples recorded after their immersion in Na_2SO_4 solution (pH 5) is presented in Fig. 5.

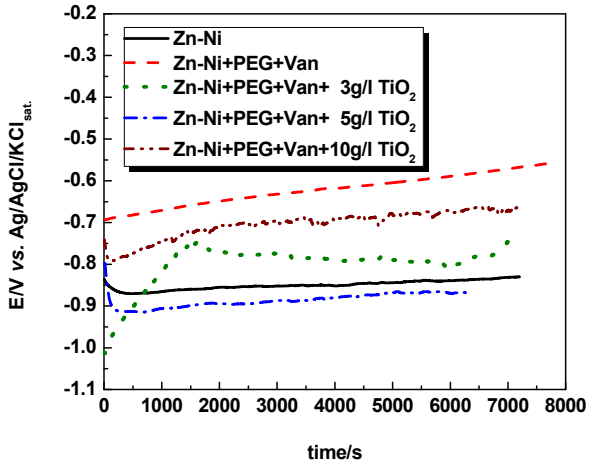

Figure 5. Evolution of open circuit potentials for Zn-Ni coatings obtained in the absence and in the presence of TiO_2 nanoparticles, after immersion in 0.2 g/l Na_2SO_4 (pH 5).

As expected, the *ocp* values noticed for Zn-Ni alloy are more positive than those observed in the same conditions for pure Zn coatings [18] suggesting a more noble character of the deposit, which could be associated to an inhibition of the anodic reaction and consequently to a higher corrosion resistance. The most positive shift was recorded in the case when only PEG and Vanillin were used, due, probably, to the smaller roughness of the surface. The fact that Zn-Ni alloys became nobler with the immersion time could be attributed to a dezincification process [19].

A shift of the *ocp* values towards more positive potentials is observed in some cases when TiO_2 nanoparticles were present in the plating bath, as compared to Zn-Ni coatings obtained without additives, suggesting an interaction of TiO_2 with the anodic reaction of the corrosion process.

Polarization curves

Polarization measurements performed in a potential range of ± 20 mV *vs. ocp* allowed the evaluation of the polarization resistance, R_p (Table 2). The higher values noticed in the presence of TiO_2 are probably due to lowering of the surface area of the electrode by embedded particles [20]. However, it should be mentioned that an increase of TiO_2 concentration beyond 3 g/l does not lead to further increase of R_p, probably due to defects and dislocations generated by the inclusion of nanoparticles in the metallic matrix.

Table 2. Polarisation resistance values calculated as the reciprocal of the slope of polarization curves (ΔE/Δi) recorded in a potential range of E = E_{corr} ± 20 mV.

Nr. crt.	Electroplating solution	R_p (Ohm)
S_{01}	Zn-Ni	8138
S_0	Zn-Ni+PEG+Van	8305
S_3	Zn-Ni+PEG+Van+TiO_2 3g/L	9995
S_5	Zn-Ni+PEG+Van+TiO_2 5g/L	9411
S_{10}	Zn-Ni+PEG+Van+TiO_2 10g/L	9033

The results of the polarization tests, carried out in a potential range of ± 200 mV *vs. ocp* using the Zn-Ni coated steel electrodes prepared in presence of different TiO_2 concentrations in the plating bath, are presented in Fig.6.

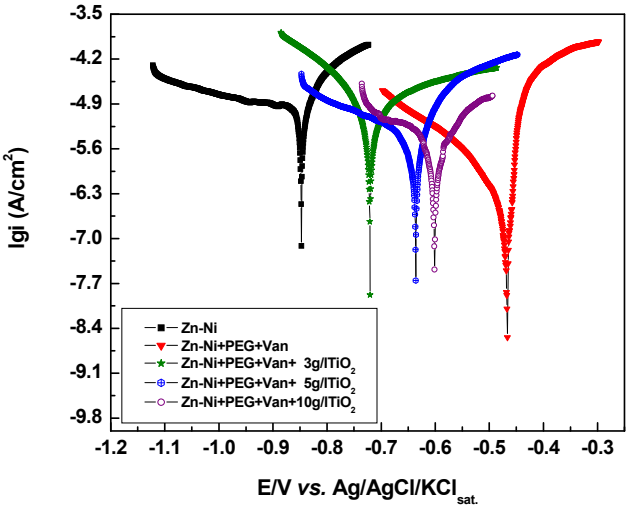

Figure 6. Polarization curve for the Zn-Ni coated steel obtained from a bath containing additives and TiO_2 nanoparticles in different concentrations. Experimental conditions: electrolyte Na_2SO_4 0.2g/l (pH=5); scan rate 0.166 mV/s; PEG, 3ml/l; Vanillin, 10 mg/l.

The corresponding corrosion reaction equations are:

$$Zn \rightarrow Zn^{2+} + 2e^-$$
$$Ni + ½\ O_2 \rightarrow NiO$$

for the anodic process, and

$$½\ O_2 + 2H^+ + 2e^- \rightarrow H_2O$$

for the cathodic one.

The values of the corrosion parameters of the coatings were calculated from the polarization curves based on the Stern - Geary theory [21], and by using Tafel interpretation (Table 3).

As it can be observed, the addition of PEG and Vanillin in the plating bath gives rise to significant decrease of corrosion current density as compared to Zn-Ni obtained without additives. This indicates that, as expected, the organic compounds strongly modified the quality of the cathodic deposit in terms of structure and morphology, producing more compact, fine-grained and consequently more corrosion resistant coatings.

In what the effect of TiO_2 nanoparticles is concerned, the addition of inert nanoparticles led to a decrease of corrosion current densities only in comparison with the pure Zn-Ni coating obtained from solution without additives. The decrease of corrosion currents could be due either to grain refinement of the deposit (see D values in Table 1), or to the fact that the incorporation of inert TiO_2 nanoparticles in the coatings isolates them from the corrosion medium and distracts the corrosion current [22].

Table 3. Kinetic parameters of the corrosion process obtained by non-linear regression using the Stern-Geary equation for interpretation of the polarization curves

Electrode	Zn-Ni	Zn-Ni +PEG+ Vanillin	Zn-Ni +PEG+ Vanillin+ 3g/l TiO_2	Zn-Ni +PEG+ Vanillin+ 5g/l TiO_2	Zn-Ni +PEG+ Vanillin+ 10g/l TiO_2
i_{corr} (A/cm^2)	$4.0*10^{-5}$	$6.3*10^{-6}$	$5.0*10^{-5}$	$2.0*10^{-5}$	$1.0*10^{-5}$
b_a* (V^{-1})	25.13	11.86	2.00	17.07	13.37
$-b_c$* (V^{-1})	2.30	2.18	10.46	4.26	13.18
E_{corr} (V/SCE)	-0.848	-0.469	-0.717	-0.646	-0.601

*b_a and b_c are the Tafel anodic and cathodic activation coefficients, respectively.

A decrease tendency of corrosion current densities of the coatings was noticed with increasing TiO_2 concentration in the plating bath. However, it should be mentioned that the differences between i_{corr} values for the samples obtained from baths containing different amounts of TiO_2 are not significant, being situated within limits of experimental errors. The acceleration of the corrosion process on Zn-Ni with additives and nanoparticles in comparison with the case of pure Zn-Ni could be due to defects and dislocations or to chemical heterogeneities generated in the metallic matrix by the embedded particles.

CONCLUSIONS

The analysis of the results led to the following conclusions:

(i) A correlation between preferred crystallographic orientation and surface morphology and of the electrodeposits was put on evidence. The platelet type grains are closely related to the (330) (or (100)) orientation.

(ii) the corrosion process on Zn-Ni-TiO_2 composite coatings is only slightly slower than on pure Zn-Ni surface and no significant decrease of corrosion current densities of the coatings were noticed with increasing TiO_2 concentration in the plating bath; this behaviour could be explained by the balance occurring between two contrary effects: on one side, the embedded inert oxide particles diminish the active surface in contact with the corrosive environment and, on the other side, they disturb the electrocrystallization process, by generating dislocations and defects in the metallic matrix which act as chemical heterogeneities and favour the corrosion process.

EXPERIMENTAL SECTION

Electrodeposition

Zn-Ni alloys were deposited from alkaline electrolytes (pH 13-14) containing 15 g/l ZnO (Merck, Germany), 130 g/l NaOH (Merck, Germany), 80 g/l triethanolamine (TEA) (Sigma-Aldrich, Germany) and 6 g/l $Ni_2SO_4*6H_2O$ (Reactivul Bucuresti). 3 ml/l Polyethylene glycol (PEG) and 10 mg/l vanillin (Sigma-Aldrich, Germany) were used as brightening agents. TiO_2 nanoparticles (99.5%, 21 nm, Degussa) were added into the plating bath in order to obtain composite Zn-Ni-TiO_2 coatings. The concentrations of TiO_2 nanoparticles were x =0 (sample S_0), x = 3 g L^{-1} (sample S_3), x = 5 g L^{-1} (sample S_5) and x=10 g L^{-1} (sample S_{10}), respectively.

Experiments were carried out in a two compartments glass cell, with the capacity of 250 ml, under magnetic stirring. The working electrode was a steel (OL 37) disk electrode, (S = 0.502 cm^2) Ag/AgCl/KCl_{sat} was used as reference electrode and a Pt foil as counter electrode. Before using, the working electrode was wet polished on emery paper of different granulation

and finally on felt with a suspension of alumina. Then, the electrode was ultrasonicated during 2 minutes, washed with acetone and distilled water in order to remove the impurities from the surface.

Corrosion measurements

For corrosion studies, a solution of 0.2 g L^{-1} $(Na)_2SO_4$ (Riedel–de Haën, Germany) (pH 5) was used.

Electrochemical measurements (open circuit potential and polarization curves) were carried out using a PC controlled potentiostat PARSTAT 2273 (Princeton Applied Research, USA). Before the polarization measurements, the open circuit potential (ocp) was recorded during 1 hour, until it was stabilized.

For evaluation of corrosion resistance, polarization measurements were carried out in 0.2g/l Na_2SO_4, using a three electrode cell. The scan rate was 0.166 mV s^{-1}, and the sweep direction was from cathodic to anodic region. Corrosion tests were conducted at room temperature.

Morphological and structural analysis

The deposit structure and the preferred orientation of crystallites were determined by X-ray diffraction (XRD) analysis, using a Brucker X-ray diffractometer with a Cu K_α (λ = 0,15406 nm) at 45 kV and 40 mA. The 2θ range of 20–100º was recorded at the rate of 0.02º and 2θ /0.5 s. The crystal phases were identified comparing the 2θ values and intensities of reflections on X-ray diffractograms with JCP data base using a Diffrac AT-Brucker program. The deposit morphology was determined with a scanning electron microscope (SEM) (Philips XL-30). The chemical composition of the nanocomposite films was determined by using an EDAX NEW XL30 (Philips) X-ray dispersive energy analyzer attached to the SEM.

ACKNOWLEDGMENTS

The authors gratefully acknowledge the financial support within the projects **POSDRU/88/1.5/S/60185** – "Innovative doctoral studies in a Knowledge Based Society" Babeş-Bolyai University, Cluj-Napoca, Romania and **PN II INOVARE No. 261/2008 (ZINITECH).**

REFERENCES

1. M.G. Hosseini, H. Asassi-Sorkhabi, H.A.Y. Ghiasvand, *Surface & Coatings Technology,* **2008**, *202*, 2897.
2. M.G. Hosseini, H. Asassi-Sorkhabi, H.A.Y. Ghiasvand, *Iranian Corrosion; ICA International Congress, Tehran: May 14-17,* **2007**.

3. G. Roventi, R. Fratesi, *Surface & Coatings Technology,* **1996,** *82*, 158.
4. M. Musiani, *Electrochimica Acta*, **2000**, *45*, 3397.
5. M. Pushpavanam, S.R. Natarajan, K. Balakrishnan, and L.R. Sharma, *Journal of Applied Electrochemistry*, **1991**, *21*, 642.
6. J. Fustes & A. Gomes & M.I. da Silva Pereira, *Journal Solid State Electrochem.,* **2008**, *12*, 1435.
7. B.M. Praveen, T.V. Venkatesha, *Applied Surface Science*, **2008**, *254*, 2418.
8. R. Ramanauskas, *Appllied Surface Science,* **1999**, *153*, 53.
9. C.G. Fink, J.D. Prince, *Transactions of the American Electrochemical Society*, **1928**, *54*, 315.
10. M. Sider, C. Fan, D.L. Piron, *Journal of Applied Electrochemistry,* **2001**, *31*, 313.
11. L.S. Tsybulskaya, T.V. Gaevskaya, O.G. Purvskaya, T.V. Byk, *Surface & Coatings Technology*, **2008**, *203*, 234.
12. Metals Handbook, 9th ed., *ASM International*, **1992**, 3.
13. F. Mansfeld, S. Gilman, *Journal of the Electrochemical Society*, **1970**, *117*, 588.
14. M.S. Chandrasekar, S. Srinivasan, M. Pushpavanam, *Journal of Solid State Electrochemistry*, **2009**, *13*, 781.
15. D.B. Lewis, C.E. Lehmberg, G.W. Marshall, *Transactions of Institute of Metal Finishing*, **2004**, *82* (1–2), 64.
16. L. Felloni, R. Fratesi, E. Quadrini, *G.* Roventi, *Journal of* Applied *Electrochemistry*, **1987**, *17,* 574.
17. E. Raub, F. Elser, Metalloberflache **1957**, *11* (5), 165.
18. M.S. Chandrasekar, S. Srinivasan, M. Pushpavanam, *Journal of Solid State Electrochemistry,* **2009**, *13*, 781.
19. D.E. Hall, *Plating & Surface Finishing*, **1983**, *70*, 59.
20. O. Kardos, D.G. Foulke, "Applications of mass transfer theory. Electrodeposition on small-scale profiles" in Advances in Electrochemistry and Electrochemical Engineering; Tobias, Ch.W.; Ed.; Publisher: Interscience New York, NY, **1966**, *2*, 145.
21. L.M. Muresan, S.C. Varvara, "Leveling and Brightening mechanisms in Metal Electrodeposition" in Metal Electrodeposition, Ed. M. Nunez, Nova Science Publishers, Inc. New York, **2005**, chapter 1.
22. M. Stern, A. L. Geary, *Journal of Electrochemical Society,* **1957**, *104*, 56.